Sequence-targeted Peptides Divert Functional Bacterial Amyloid Towards Destabilized Aggregates and Reduce Biofilm Formation

Thorbjørn V. Sønderby [1,2], **Nikolaos N. Louros** [3,4], **Ladan Khodaparast** [3,4], **Laleh Khodaparast** [3,4], **Daniel J. Madsen** [1], **William P. Olsen** [1,2], **Nele Moonen** [3,4], **Madhu Nagaraj** [1], **Vita Sereikaite** [5], **Kristian Strømgaard** [5], **Frederic Rousseau** [3,4], **Joost Schymkowitz** [3,4] **and Daniel E. Otzen** [1]*

1 - *Interdisciplinary Nanoscience Center (iNANO),* Aarhus University, Gustav Wieds Vej 14, 8000 Aarhus C, Denmark

2 - *Sino-Danish Center (SDC),* Eastern Yanqihu Campus, University of Chinese Academy of Sciences, 380 Huaibeizhuang, Huairou District, Beijing, China

3 - *Switch Laboratory,* VIB-KU Leuven Center for Brain and Disease Research, Herestraat 49, 3000 Leuven, Belgium

4 - *Switch Laboratory,* Department of Cellular and Molecular Medicine, KU Leuven, Herestraat 49, 3000 Leuven, Belgium

5 - *Department of Drug Design and Pharmacology,* University of Copenhagen, 2100 Copenhagen Ø, Denmark

Correspondence to Daniel E. Otzen: dao@inano.au.dk *(D.E. Otzen)* @tvs1212 🐦 *(T.V. Sønderby),* LourosNikos 🐦 *(N.N. Louros),* @LadanKhodapara1 🐦 *(L. Khodaparast),* @LalehKhodapara1 🐦 *(L. Khodaparast),* @vitasereikaite 🐦 *(V. Sereikaite),* @stromgaardlab 🐦 *(K. Strømgaard),* @VIB_Switch_Lab 🐦 *(F. Rousseau),* @VIB_Switch_Lab 🐦 *(J. Schymkowitz),* @daniel_otzen 🐦 *(D.E. Otzen)*
https://doi.org/10.1016/j.jmb.2023.168039
Edited by Sheena Radford

Abstract

Functional bacterial amyloid provides structural stability in biofilm, making it a promising target for anti-biofilm therapeutics. Fibrils formed by CsgA, the major amyloid component in *E. coli* are extremely robust and can withstand very harsh conditions. Like other functional amyloids, CsgA contains relatively short aggregation-prone regions (APR) which drive amyloid formation. Here, we demonstrate the use of aggregation-modulating peptides to knock down CsgA protein into aggregates with low stability and altered morphology. Remarkably, these CsgA-peptides also modulate fibrillation of the unrelated functional amyloid protein FapC from *Pseudomonas,* possibly through recognition of FapC segments with structural and sequence similarity with CsgA. The peptides also reduce the level of biofilm formation in *E. coli* and *P. aeruginosa,* demonstrating the potential for selective amyloid targeting to combat bacterial biofilm.

Introduction

Amyloids are fibrillar protein aggregates rich in β-sheet secondary structure.[1,2] The β-strands are stacked on top of each other perpendicular to the fibril spine to form a characteristic structure called a cross-β spine.[1,2] The residue side chains involved in the cross-β spine are tightly interlaced into so-called steric zippers, leading to a very stable struc-ture.[3] Amyloids have been extensively studied since the discovery of their role in neurodegenerative diseases such as Parkinson's and Alzheimer's diseases.[1,4,5] Amyloid that accumulates in disease is considered a result of protein misfolding and is often formed by intrinsically disordered proteins (IDP).[1] However, amyloids are not always associated with disease. So-called functional amyloids perform functional roles in organisms and are espe-

cially abundant in bacteria.[6–9] The roles of functional bacterial amyloids (FuBA) include surface adhesion properties and structural support in biofilm.[6–9] The first discovered FuBA is curli from *Escherichia coli* (*E. coli*).[6] The main structural curli-component, CsgA, can be purified from bacteria and fibrillates readily *in vitro*.[11,11] CsgA fibrils formed *in vitro* are identical to curli fibers formed *in vivo*.[11] However, the *in vivo* biogenesis of curli, which leads to fibrils extending from the outer membrane of *E. coli*, requires six other helper proteins transcribed from two operons (csgBAC and csgaDEFG).[13] The roles of the helper proteins include transcription regulation (CsgD),[14] chaperones (CsgC, CsgE and CsgF)[15–17] and an outer membrane pore protein (CsgG).[18] CsgA is an IDP and is secreted to the cell surface where its fibrillation is nucleated by CsgB.[14,18] CsgA consists of five imperfect repeat sequences that are each ~22 residues long. In the folded state of CsgA, each repeat sequence is predicted to form two β-strands connected by a β-turn.[20,20] The repeats stack on top of each other, resulting in a β-helix.[21,21] The fibrillation of CsgA is remarkably robust and tolerates an extremely wide span of pH values[12]; it can even take place at high concentrations of denaturant.[23] CsgA is not harmful to the organism despite its efficient aggregation.[24] This is believed to be largely thanks to the helper proteins which stringently control the safe biogenesis of curli by keeping CsgA unfolded until it reaches the cell surface.[15–17] In addition, the three middle repeats, R2-R4, contain gatekeeper Asp and Gly residues which reduce the aggregation propensity of CsgA.[24] Curli is involved in biofilm formation[6,19] and harbors several virulence features.[20,24,25] These features make curli a promising target for anti-biofilm therapeutics.

Amyloid cores are formed from aggregation-prone regions (APR) in the primary sequence of proteins.[27] Such APRs may be predicted using dedicated algorithms which identify the most probable positions of the amyloid cross-β spine.[27–30] Peptides targeted against protein APRs can modulate protein fibrillation through different mechanisms, including seeding,[31] heterotypic aggregation or fibril-end capping caused by steric hindrance or charge repulsion.[32] Interestingly, most proteins, including proteins normally considered non-amyloidogenic, contain at least one APR which is typically buried in the hydrophobic core of the protein upon folding. Peptides targeted against these APR can lead to a precipitation of the protein through interference with folding and subsequent precipitation.[31,32,33] Similar APRs may be shared by multiple proteins within a proteome, allowing the precipitation of multiple proteins using one peptide.[31] Previous work has highlighted that tandem peptides targeting redundant APRs found in many bacterial proteins show a remarkable antimicrobial effect.[31,34,35] Notably, the APRs in target proteins do not necessarily have to perfectly match the APR of the aggregation-inducing peptide, but tolerate a degree of mismatch.[31]

Here, we provide a new twist to this tale by using peptides to target APRs of a naturally aggregating protein, not to direct it from the folded to the aggregated state, but rather to divert it away from the functionally aggregated state into an inactive precipitated form. We find that peptides targeting the functional amyloid protein CsgA induce a rapid precipitation of CsgA, leading to aggregates with a markedly different morphology compared to naive CsgA fibrils. In addition, we show that the rapidly formed aggregates are significantly less stable than non-treated amyloids. Further, we demonstrate that the interaction between CsgA and peptides that share APRs with the terminal repeats of CsgA is dependent on Arg residues. In addition, we show that CsgA-derived peptides can modulate the fibrillation of the FapC protein in *Pseudomonas aeruginosa* (*P. aeruginosa*), possibly because of similarities in sequence and structure between FapC and CsgA APRs. Finally, we demonstrate that several of our peptides reduce the biofilm formation of *E. coli* and *P. aeruginosa*. Thus, the strategy of targeting APRs for protein precipitation can be extended to an already aggregation-prone protein to lead to loss of function.

Results and Discussion

Implementing peptide arrays to identify CsgA-interacting regions

We constructed a peptide microarray library containing the entire sequence of CsgA displayed in 14-mer peptides that were printed on a Celluspot glass slide. To investigate CsgA-CsgA interactions, we incubated our peptide array, containing displayed CsgA segments, with Alexa Fluor546-labelled (A546) full-length CsgA. Notably, CsgA protein showed strong interactions with peptides located in the R1 and R5 terminal repeat regions (Supplementary Figure S1(a)). We also observed CsgA interactions with peptides located in the R3, and to a lesser extent, in the R4 region. No peptides derived from the R2 region showed any strong interactions with CsgA, potentially as an effect of the reduced tendency of association in repeats containing Asp and Gly gatekeeper residues.[24]

Complementary peptide design strategies targeting terminal repeats of CsgA

Based on our microarray data, the R3 and terminal R1 and R5 repeats appeared to be the most promising intrinsic sequences as putative drivers of CsgA-CsgA interactions. In order to reduce the sequence search space for targets against CsgA, we subsequently decided to focus primarily on APRs contained within the terminal

repeats of CsgA. This decision was based on the following: (i) computational analysis of the aggregation profile of CsgA revealed that R1 and R5 contain some of the most identifiable aggregation-prone stretches (Figure S2(a,b)), (ii) the same regions identified in (i) have been previously experimentally verified to form amyloid-like aggregates[37,37] and (iii) several lines of evidence indicate that CsgA potentially adopts a β-solenoid-like fold that supports its axial proliferation into curli amyloid fibrils through successive stacking interactions that take place between the terminal R1 and R5 repeats.[39–41]

A peptide library aimed at targeting these interaction interfaces was generated using three main rational design strategies (Figure S3). Firstly, we synthesized analogs of both terminal regions, as well as positional variants incorporating gatekeeper mutations within their corresponding APR regions that could potentially still interact with the solenoid edge surface, yet possibly block further axial elongation (P9-17, Strategy 1). In a series of recent findings, we showed that tandem designs targeting potent APRs were extremely effective in the development of aggregation-based anti-bacterial and anti-viral peptide designs.[31,34,41] Following this premise, we generated a list of similar designs (Strategy 2), by alternating gatekeeper and linker residues, targeting the strongest APRs identified for R1 and R5, respectively (peps 18–29). Furthermore, in Strategy 3, we also utilized a structure-based approach to target the same APR regions of R1 and R5[32] (P30-61, cf. Figure S2(cd)). Briefly, we used as templates the solved three-dimensional structure of the $_{135}VNVTQV_{140}$[38] amyloid fibril as well as structural models produced by Cordax[29] for $_{43}SELNIY_{48}$ and $_{55}SALALQ_{60}$. We performed thermodynamic calculations using the derived template structures and the FoldX force field[45] in order to identify sequence variants that were calculated to interact with the given sequences with cross-interaction energies that are more favorable than their WT sequence counterpart (peps 30–61). Finally, we complemented our designs by adding peptide analogs corresponding to the signal peptide (directing CsgA across the inner membrane) and the N22-sequence (which directs CsgA to the CsgG export system in the outer
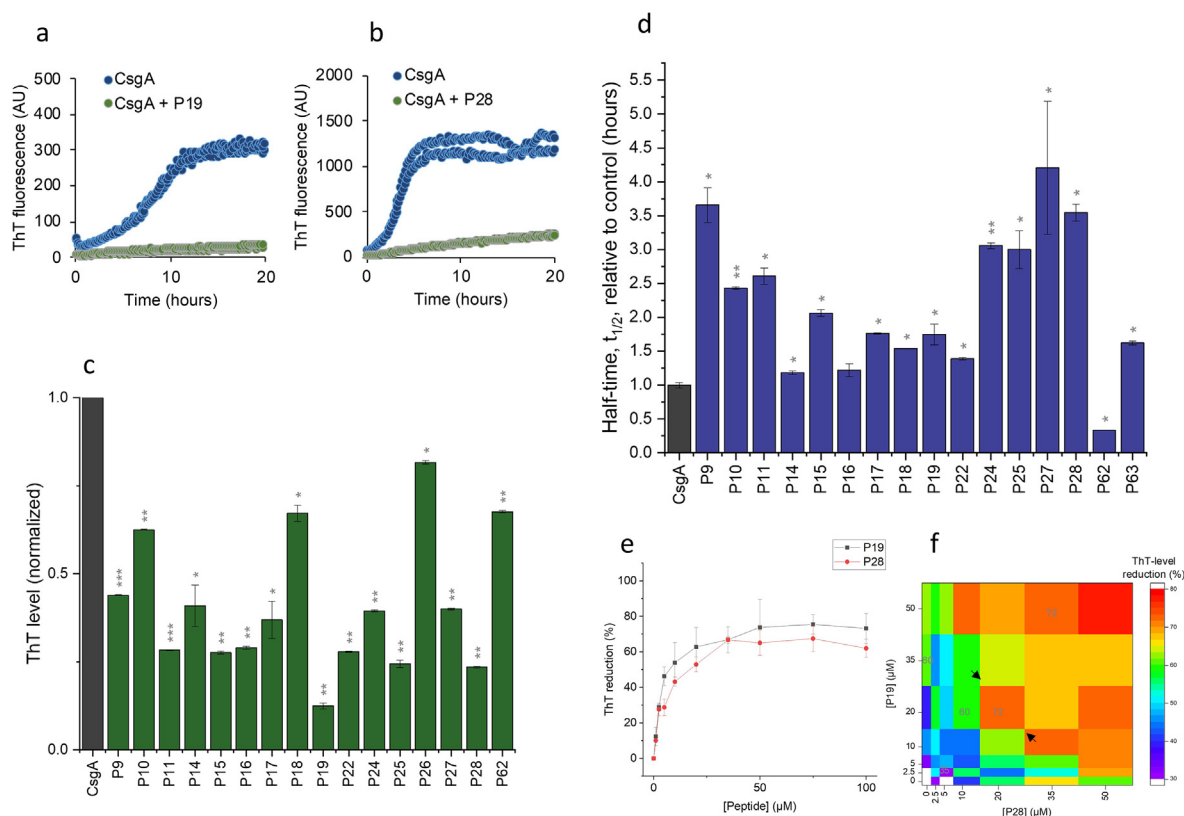
Figure 1. Screening of first-generation peptides showing modulation of CsgA fibrillation. CsgA fibrillation curves in the absence and presence of peptide P19 (a) or P28 (b). (c) ThT end-level of CsgA fibrillation in presence of peptides. (d) Fibrillation half-times ($t_{1/2}$) of CsgA fibrillation in presence of peptides. (e) Dose-response curves showing the peptide-induced reduction in ThT end-level (%) measured relative to untreated CsgA. (f) Heatmap showing the reduction in ThT end-level of CsgA fibrillation in presence of various concentrations of P19 and P28. Error bars are standard deviation (negative controls, n = 4, samples, n = 2), and *, ** and ***, denotes a *p* value of ≤ 0.05, ≤ 0.01 and ≤ 0.001, respectively.

membrane).[46] Each repeat region of CsgA was also synthesized, except R1, which our supplier was not able to synthesize, possibly because of its high aggregation propensity. Instead, four destabilized variants of R1 were synthesized (R1_mut1-4), which contained 3–4 positively charged gatekeeper mutations.

Fibrillation of CsgA is modulated by CsgA-targeted peptides

To experimentally test if the designed peptides showed any modulating effect on CsgA fibrillation, we synthesized a library of 63 CsgA-derived peptides and recombinantly expressed and purified full-length CsgA protein. Each peptide was mixed with full-length CsgA in the mass ratio 1:1 and the fibrillation of CsgA was monitored using ThT assays (Figure 1(a,b) and Figure S4). We also checked for self-fibrillation of all peptides in the absence of CsgA (Figure S5). Eleven peptides fibrillated on their own, including the predicted aggregation-prone repeat sequence analogs, R1 (mut4), R3 and R5. The less aggregation-prone R4 repeat also self-fibrillated but only after a long lag phase. The aggregation propensity of the repeat sequences, therefore, perfectly matched our observations from our peptide array, which showed high CsgA protein-CsgA peptide interactions in R1, R3 and R5 and less interaction in R4, but no interaction in R2. The self-fibrillating peptides were not analyzed further. Of the rest, 13 peptides reduced the ThT fluorescence level markedly (to less than 50% of control ThT-level) (Figure 1(c)), suggesting that the extent of CsgA amyloid formation was reduced by these peptides. In addition, the CsgA fibrillation half-time (time to reach half maximum fluorescence) was increased 2-fold or more by eight peptides (Figure 1(d)). To investigate if the reduction in ThT level was caused by a lower amount of aggregated CsgA monomer rather than *e.g.* changes in the structure of the aggregates, we analyzed the supernatant of the samples using sodium dodecyl sulphate polyacrylamide gel electrophoresis (SDS-PAGE). Protein converted to functional amyloid is SDS-insoluble, and any soluble protein in the samples is expected to be monomeric.[23] However, no monomeric CsgA was present in the samples, which indicated that the CsgA protein was aggregated even in the presence of peptides (Figure S6), but presumably to another kind of (less ThT-binding) aggregate.

We concentrated our efforts on the two peptides which reduced the ThT level of CsgA to the greatest extent, namely P19 and P28. P19 and P28 are both APR tandem repeats flanked by positively charged Arg gatekeeper residues. P19 is targeted against CsgA's first repeat (R1) and hence contains the APR of R1, whereas P28 is targeted against R5 and contains the APR of R5. They also differ in their linkers; P19 contains a rigid PP linker whereas P28 contains a flexible GS linker. First, we measured the reduction in fibrillation ThT end-level of 7 μM CsgA at increasing concentrations of P19 or P28 (Figure 1 (e)). The response saturated at ~35 μM P19 or P28, corresponding to molar CsgA:P19 and CsgA:P28 ratios around 1:5. When the slope of the dose–response curve at low [P] was extrapolated to the saturation plateau level we observe an intercept at ~7 μM (Figure S7(a)), corresponding to a stoichiometry at approximately 1:1 for both
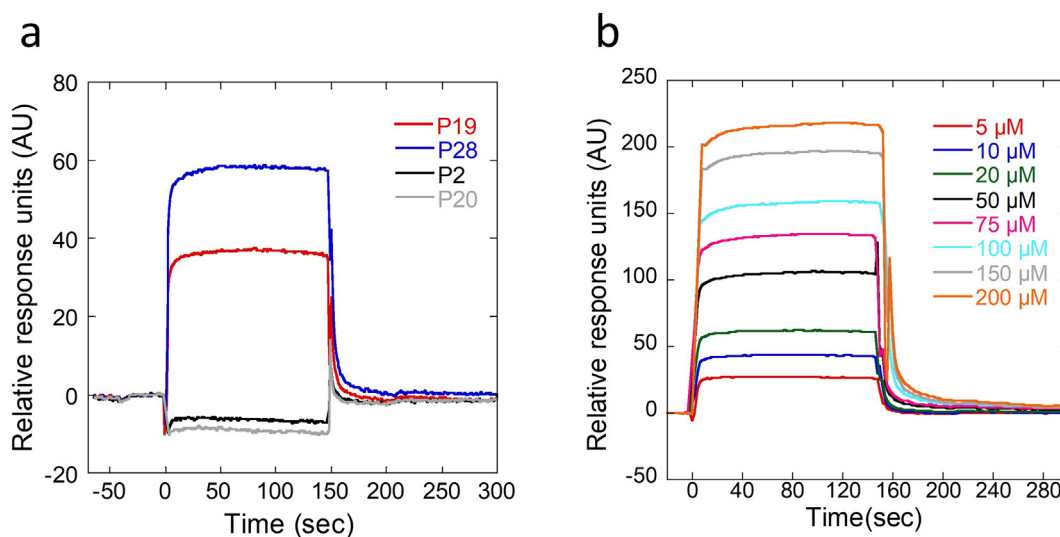
Figure 2. Comparison of the interaction between peptides and CsgA (a) SPR sensorgrams showing the interaction between CsgA and either P19 or P28. The negative controls P2 and P20 showed no interaction with CsgA. (b) Sensorgrams of the interaction between P19 (5–200 μM) and CsgA.

CsgA:P19 and CsgA:P28. Previous studies of similar peptides, designed by the same tandem repeat principle, have suggested the presence of small seeds which interact with target proteins.[36] Transmission Electron Microscopy (TEM) analysis of P19 and P28 indicated that seed-like aggregates were present (Figure S8). Next, we investigated potential synergy between P19 and P28 by co-incubating CsgA with various combinations of [P19] and [P28]. The relative reduction in ThT-level was plotted in a heatmap (Figure 1(f)). A distinct "ridge" is observed in the heatmap starting at
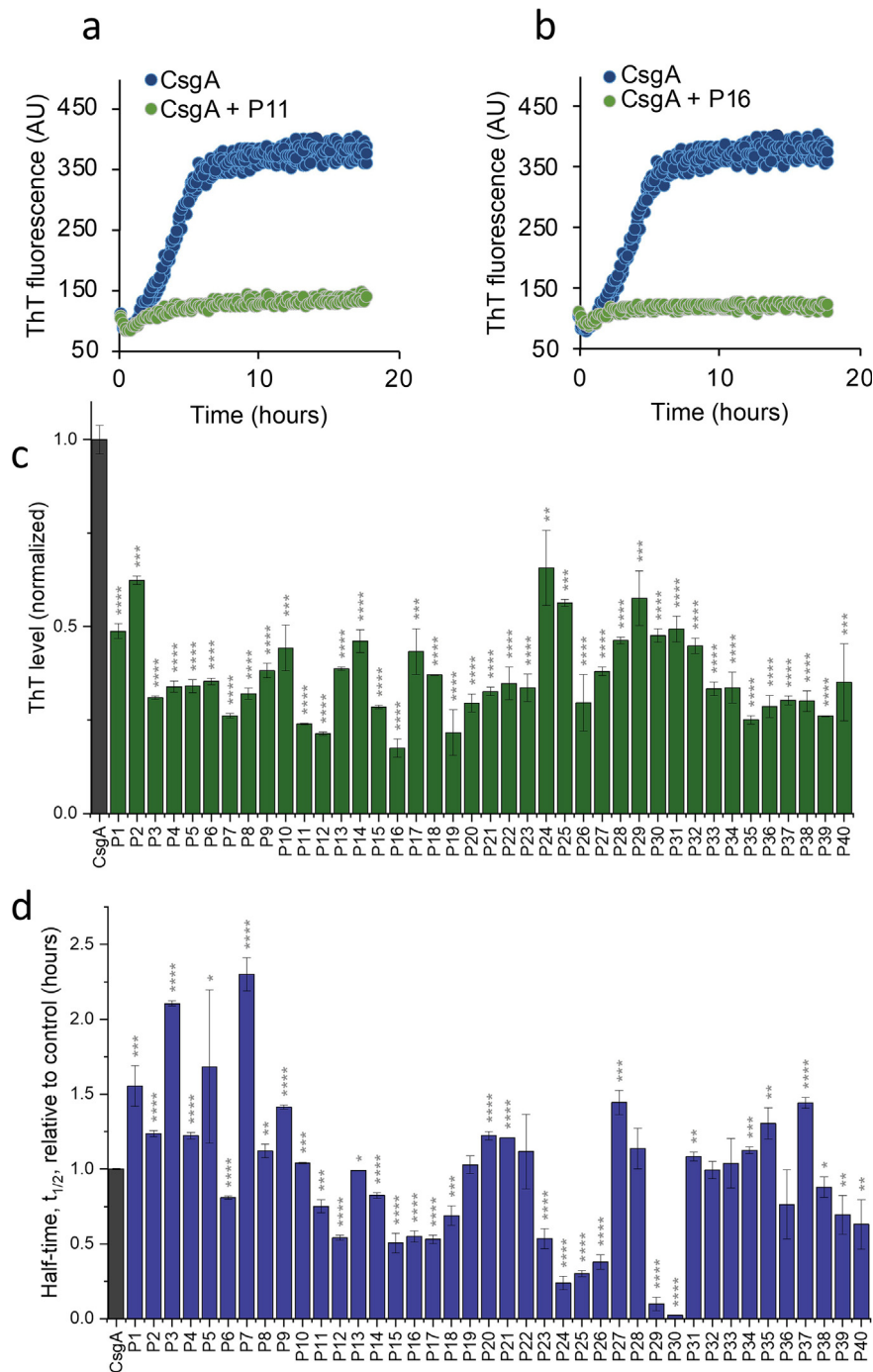
Figure 3. Screening of second-generation peptides showing modulation of CsgA fibrillation. (a) CsgA fibrillation curves in the absence and presence of peptide P11 (a) or P16 (b) from the second peptide generation. (c) ThT end-level of CsgA fibrillation in presence of peptides. (d) Fibrillation half-times ($t_{1/2}$) of CsgA fibrillation in presence of peptides. Error bars are standard deviation (negative controls, n = 4, samples, n = 2), and *, **, *** and **** denotes a p value of ≤ 0.05, ≤ 0.01, ≤ 0.001 and ≤ 0.0001, respectively.

$\sim$20 μM P19 and $\sim$20 μM P28 (as indicated by the black arrow in Figure 1(f)). The ThT reduction obtained by combining 20 μM P19 and P28 is more pronounced than CsgA co-incubated with 40 μM of either P19 or P28, which indicates a degree of synergy between the peptides. This is a likely scenario since P19 and P28 are targeted against each of their terminal repeat of CsgA which are expected to gain intermolecular contact during fibrillation.[21]

Next, we investigated the interaction between CsgA and peptides using Surface Plasmon Resonance (SPR) (Figure 2). CsgA monomers were immobilized on the SPR chip and the interaction between peptides and CsgA was measured. As expected, P19 and P28 interacted with the immobilized CsgA (Figure 2(a)). As negative controls, we selected two peptides, P2 and P20, which showed no effect in our fibrillation ThT assays (Figure S5). In agreement with our fibrillation data, P2 and P20 showed no interaction with CsgA on the SPR chip (Figure 2(a)). The binding of P19 and P28 to CsgA was concentration-dependent (example shown for P19 in Figure 2(b)), with a dissociating constant in the micromolar range (90 μM) (Figure S7(b)). These results confirm that modulation of aggregation by peptides is due to interactions between peptides and CsgA.

A new generation of peptides revealed a robust design that consistently lowered the ThT signal

In a secondary effort to improve the designs of our initial peptide hits, we generated a second round of rational designs based on P19 and P28 (Figure S9 and Table S2). In this second generation, we produced hetero-tandem versions of the initial hits which target both R1 and R5. The initial hits were designed to target APRs of either R1 and R5 in a homo-tandem setup. As with the initial screen, we coupled this approach once more to designs incorporating linkers of various lengths, rigidity and physicochemical properties. Finally, we further included mutated variants by incorporating residues linked to strong axial aggregation blocking efficiencies (positive charges and bulky aromatic side chains), as shown by previous work by us[32] and others.[47,45]

We tested the new peptide library on CsgA fibrillation (Figure 3(a,b) and Figure S10). All peptides reduced the CsgA ThT end-level, indicating a robust design strategy (Figure 3(c)). However, the new peptide library did not reduce ThT end-level more than P19 and P28 from our first library. Interestingly many of the new peptides showed lower half-time compared to non-treated CsgA fibrillation (Figure 3(d)), indicating that the peptides rapidly diverted CsgA into an alternate aggregate.

Peptides induce the formation of CsgA aggregates with different morphology and low stability

To further investigate the peptide-induced aggregation response, we measured the turbidity of CsgA mixed with peptides (Figure 4(a)). Several samples showed high turbidity immediately after mixing peptides and CsgA, which indicated that these peptides induced fast precipitation of aggregation CsgA. The rapid increase in turbidity was especially prominent for second-generation peptides (peptides labeled with the extension -r2). This indicated that the modifications added to the second-generation peptides induced a fast aggregation response. This precipitation of CsgA is probably similar to the peptide-induced precipitation of many soluble proteins in the proteome of *E. coli*.[31]

Since CsgA is functional in its fibrillated state, loss of functionality of CsgA aggregates requires the peptide-modulated CsgA aggregates to differ from naïve CsgA fibrils, *e.g.* in terms of structure or stability. To address this, we first analyzed the aggregates formed in presence of peptides by TEM and found them to be markedly different in morphology from the thin, regular and well-dispersed fibrils formed by CsgA on its own (Figure 4(b)). Complexes formed in the presence of fibrils ranged from twisted and highly bundled short fibrils (P28) to very stumpy small fibrils (P11-r2), irregular rhomboids (P16-r2) and even small spherical structures (P19).

Secondly, we turned to stability measurements. Besides morphology, another important feature of functional amyloid is their extreme stability. They withstand high concentrations of denaturant[23] and require high concentrations of formic acid to be dissolved.[49] Indeed, the response to formic acid can be modelled analogously to unfolding of globular proteins in denaturants, since incubation of CsgA aggregates in increasing concentration of formic acid leads to a sigmoidal denaturation response (Figure 4(c) inset). Our previous studies of formic acid-induced protein denaturation demonstrated that this method is useful for assessing the stability of functional amyloid.[49] We screened the solubility of peptide-modulated CsgA aggregates in 50% formic acid, a concentration where ca. 20% of wt CsgA is solubilized (Figure 4(c)). Most of our peptides increased CsgA solubility significantly, indicating reduced stability of the CsgA-peptide aggregates. Among the first-generation peptides, P53, which leads to very rapid CsgA aggregation, also led to the highest solubility, indicating that P53 efficiently diverts CsgA towards much less stable complexes. There is however no simple pattern to this effect. The effect was seen for some round 1 peptides and all of the six tested round 2 peptides, in addition to the hexapeptide P53. Nevertheless, we noted a correlation between turbidity at 0 h and rapid aggregation. Peptides with high turbidity at 0 h generally

showed short half-times in the ThT assays and conversely peptides with low turbidity at 0 h had long fibrillation half-times in the ThT assays (Figure 4 (d)). Furthermore, 0 h turbidity also correlated positively with solubility in formic acid (Figure S11). This suggested that fast induction of aggregation by peptides partitions CsgA into kinetically accessible but thermodynamically not very stable aggregates.

What sequence features are responsible for this effect? Peptides causing high turbidity at 0 h contained a higher number of Arg residues compared to the low-turbidity peptides (Figure 4 (d)), suggesting an importance of Arg residues in rapid precipitation of CsgA. Two of the high-turbidity peptides also contained Trp residues but this was not a prerequisite for higher turbidity
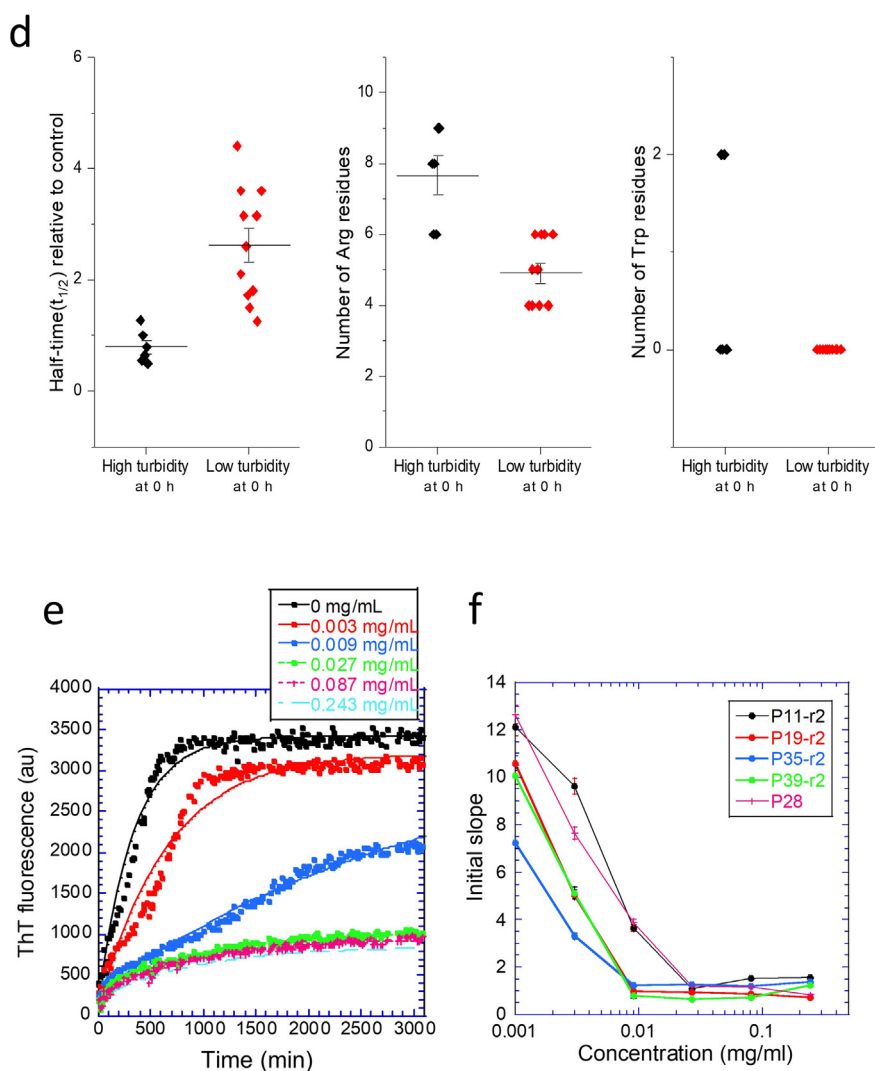

b

CsgA   CsgA + P19   CsgA + P28   CsgA + P11-r2   CsgA + P16-r2

c
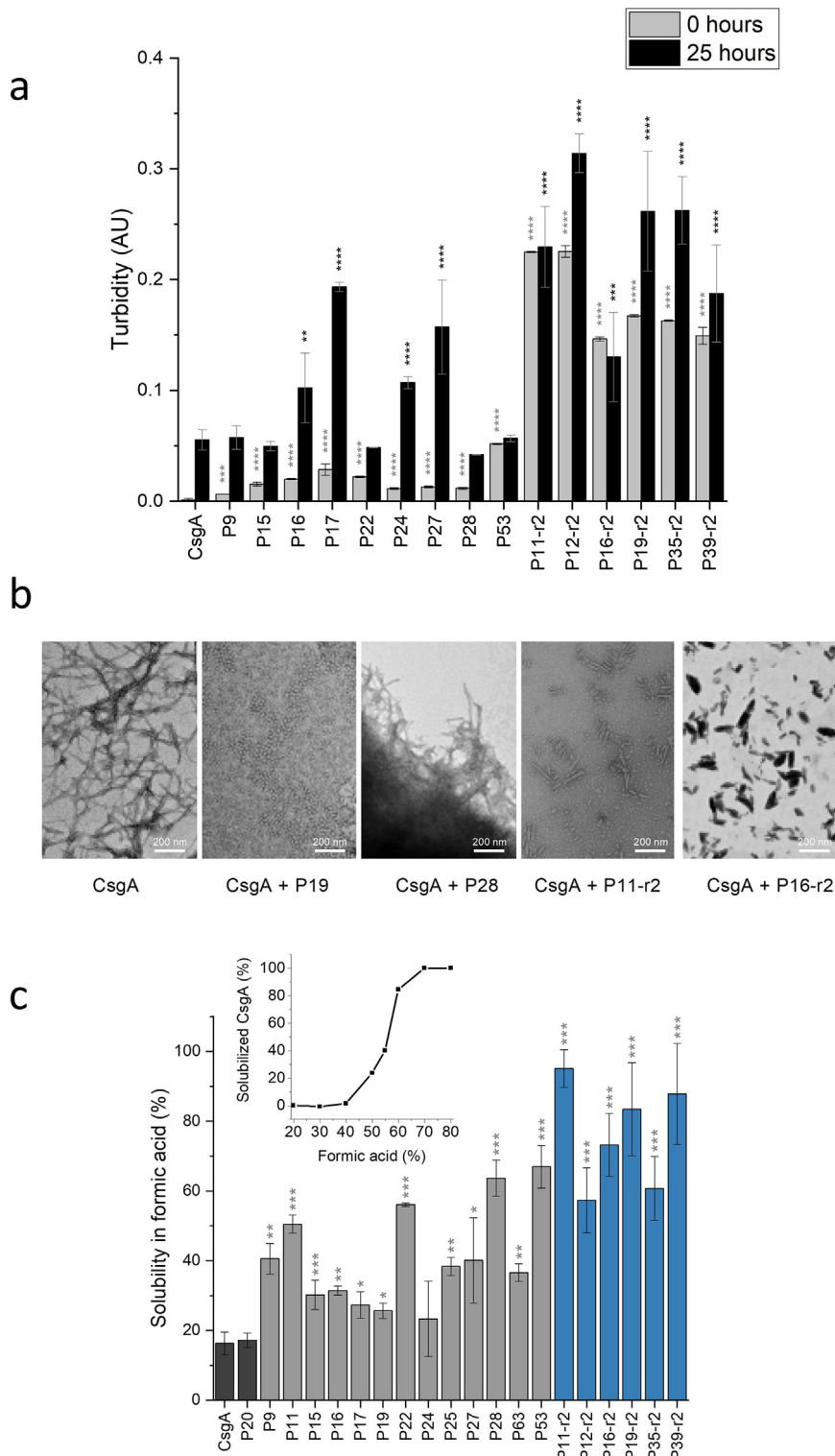
Fig 4. *(continued)*

(Figure 4(d)). Interestingly, the majority of the high-turbidity peptides were hetero-tandem peptides, containing one R1 APR and one R5 APR, while the remaining homo-tandem peptides were based on R5 APR (Table 1). No high-turbidity peptides were solely based on R1 APR. This is in agreement with our synergy analysis which suggested that a combined use of R1 and R5 APRs is ideal for effective ThT-reduction (Figure 1 (f)). The type of linkers in the tandem peptides that led to the highest reduction in ThT level appeared to be either Pro-Pro or Gly-Ser with a majority of the high-turbidity peptides containing the latter. The choice of linker did not appear to be a major determinant for the induction of high turbidity at 0 h, because the low-turbidity peptides

Figure 4. Comparison of peptide-induced aggregation. (a) Turbidity (600 nm) as measured for CsgA samples mixed with peptides at 0 h and 25 h. (b) TEM image of CsgA aggregates in the absence or presence of either P19, P28, P11-r2, or P16-r2. (c) Solubility (%) of CsgA aggregates dissolved in formic acid (50% v/v). The aggregates were formed in the absence or presence of peptides. Inset: Representative sigmoidal curve showing the solubility of CsgA as a function of formic acid (%). (d) Comparison of peptides causing high or low turbidity at 0 h in (a), with regards to half-time ($t_{1/2}$) (left panel), number of Arg residues (middle panel) and number of Trp residues (right panel). (e) Seeded CsgA fibrillation curves in the presence of increasing peptide concentration (in this case fibrillation curves in presence of P28 is shown as a representative example). (f) The initial slope of the seeded CsgA fibrillation in presence of five different peptides is plotted as a function of peptide concentration. Error bars are standard deviation (negative controls, n = 4, samples, n = 2), and *, **, *** and **** denotes a *p* value of ≤ 0.05, ≤ 0.01, ≤ 0.001 and ≤ 0.0001, respectively.

Table 1 Comparison of peptides resulting in low or high turbidity of CsgA samples at 0 h.

Peptide	Sequence	Peptide type	Turbidity at 0 h
P9	SRLRIRQRGGGNSALALQDARN	R1 mutants	Low
P11	SELNIYQYGGGRSRLRLRDARN	R1 mutant	
P15	SSRNRTRVRFGNNATAHQY	R5 mutant	
P16	SSVNVTQVRFRNRARAHQY	R5 mutant	
P17	SSVNVTQVGRGRNRTRHQY	R5 mutant	
P19	RSELNIYQRRPPRSELNIYQRR	Tandem APR peptides (R1)	
P22	RSELNIYQRRGSRSELNIYQRR	Tandem APR peptides (R1)	
P24	RSVNVTQVRPPRSVNVTQVR	Tandem APR peptides (R5)	
P27	RSVNVTQVRGSRSVNVTQVR	Tandem APR peptides (R5)	
P28	RSVNVTQVRRGSRSVNVTQVRR	Tandem APR peptides (R5)	
P53	VNVRQV	Hexapeptide (R5)	Medium
P11-r2	RSRLRIRQRRPPPRSRLRIRQRR	Tandem APR peptides (R1/R5)	High
P12-r2	RSVNVTQVRRPPRSRLRIRQRR	Tandem APR peptides (R5/R1)	
P16-r2	RSVNVTQVRRPPRSWLWIYQRR	Tandem APR peptides (R5/R1)	
P19-r2	RSELNIYQRRGSRSVRVRQVRR	Tandem APR peptides (R1/R5)	
P35-r2	RSVRVRQVRRGSRSVNVTQVRR	Tandem APR peptides (R5)	
P39-r2	RSVWVWQVRRGSRSVNVTQVRR	Tandem APR peptides (R5)	

contained a relatively similar amount of Pro-Pro and Gly-Ser linkers.

Peptides effectively reduce seeded fibrillation

To investigate if the peptides block axial aggregation, we turned to seeded fibrillation. In the absence of peptides, the addition of 5% w/w seeds led to an immediate fibrillation growth response (Figure 4(e)). However, increasing the concentration of peptides from 0 to 0.24 mg/mL led to an efficient suppression of the fibrillation growth as shown by the ~10-fold reduced initial slope of the growth curve (data for P28 shown in Figure 4(e); summary in Figure 4(f)). These results indicated that the peptides associate with fibril ends and block further association of monomers with the fibril ends.

Aggregation prone segments of CsgA share similarities with FapC from Pseudomonas aeruginosa

Given the high effectiveness of our peptides against CsgA fibrillation *in vitro*, we turned to biological assays to test the potential of our peptides for anti-biofilm treatment. As mentioned previously, tandem peptides targeting a single APR found in multiple proteins with one peptide can induce aggregation of multiple target proteins in bacteria, demonstrating antimicrobial potential.[31,34,35] We therefore performed a bioinformatic search for CsgA-like APRs in the proteomes of *E. coli* and *P. aeruginosa*. We limited our analysis to proteins that showed a similarity with the APRs of R1 and R5. We noticed a similarity between R1 and R5 segments in CsgA and three segments of the protein FapC in *P. aeruginosa* (Figure 5(a)). Intriguingly, FapC is a functional amyloid similar to CsgA but the two proteins are evolutionarily unrelated.[7] The three segments that we identified in FapC are

predicted to be core segments in FapC fibrils according to multiple amyloid prediction algorithms,[50] and mutagenesis of the segments significantly decelerates fibrillation of FapC.[50] This is supported by the FapC structure predicted by AlphaFold,[51,49] where these three segments are predicted to stack on top of each other to form a cross-β backbone (Fig. 5b) (UNIPROT ID: Q9I2F0). Next, we set out to investigate if these partially shared segments of CsgA and FapC allowed for interaction between CsgA-targeted peptides and FapC. We recombinantly expressed and purified FapC protein from *Pseudomonas sp.* UK4, which is shorter than PAO1 FapC but maintains the three segments of interest.[7] To test for a potential cross-interaction between FapC and CsgA-derived peptides, we focused on a 6-residue APR segment of CsgA, VNVTQV, which readily forms fibrils *in vitro*[37] suggesting that this APR is a core segment of CsgA fibrils. We synthesized a destabilized version of VNVTQV, P53, where Thr in position 4 is substituted by Arg, which abolishes the peptide's fibrillation propensity (Figure 5(c)). Nevertheless, when P53 was mixed with CsgA, an almost immediate increase in ThT-level was observed, which indicated that P53 interacted with CsgA, possibly through heterotypic aggregation or cross seeding which may be templated by the cross-β spine of the full-length CsgA protein (Figure 5(c)). Next, we investigated if UK4 FapC was able to interact with the CsgA R5 hexapeptide, P53. When we mixed P53 with FapC, ThT fluorescence immediately increased just as with CsgA, suggesting an interaction between FapC and P53 (Figure 5(c)). This interaction may be explained by a 3-residue overlap in the APR-region of PAO1 FapC and P53. Indeed, when P53 in a predicted β-strand conformation is overlaid with the AlphaFold-predicted[9,39] structure of the PAO1 FapC APR-region, a match is seen between the conserved
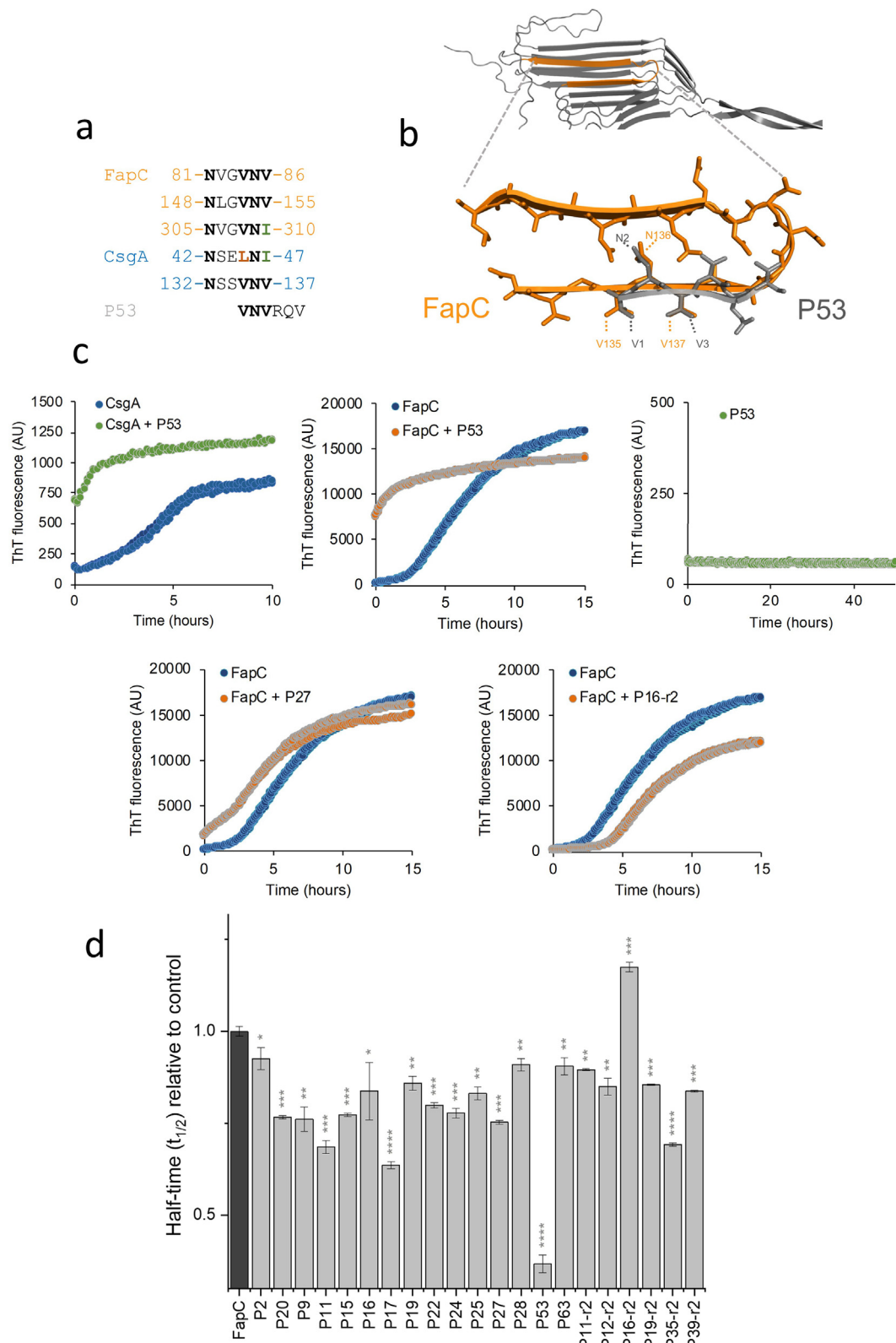
Figure 5. Modulation of FapC fibrillation using CsgA-targeted proteins. (a) Sequence similarity between conserved segments of FapC and CsgA. (b) Sequence- and structural similarity between P53 and a predicted aggregation-prone region of FapC. (c) CsgA and FapC fibrillation curves in the absence and presence of peptide P53, P27 and P16-r2. (d) Fibrillation half-times ($t_{1/2}$) of FapC fibrillation in presence of peptides. Error bars are standard deviation (negative controls, n = 4, samples, n = 2), and *, **, *** and **** denotes a *p* value of ≤ 0.05, ≤ 0.01, ≤ 0.001 and ≤ 0.0001, respectively.

135-VNV-137 region of FapC and P53 (Figure 5(a, b)), suggesting potential for cross-interaction. Motivated by this observation, we screened additional peptides (Figure 5(c) and Figure S12). Although no peptide had such a dramatic effect on FapC aggregation as P53, several CsgA-targeted peptides led to either reduced or increased half-times (Figure 5(d)). We investigated the interaction between UK4 FapC and the CsgA-targeted peptides, P19 and P28 using SPR. Strikingly, both P19 and P28 interacted with FapC (Figure S13), suggesting that the identified APR sequence similarity between CsgA and UK4 FapC allows interaction between CsgA-targeted peptides and FapC. To investigate whether this shared susceptibility to certain peptides could reflect a potential cross-seeding between CsgA and FapC, we added CsgA seeds to monomeric FapC (Figure S14). Although CsgA seeds led to a slightly earlier onset of ThT-increase, the effect was modest compared to unseeded FapC fibrillation and suggested a limited interaction. We consider it more likely that FapC-CsgA cross-interaction may involve shorter segments of the two proteins.

To further map the interactions between FapC protein and CsgA peptides, we incubated A546-labelled FapC with our CsgA peptide library array (Figure S1(b)). Remarkably, we observed substantial overlap in the binding areas of FapC and CsgA protein to CsgA peptides, demonstrating several shared peptide binding partners as indicated from our SPR experiments and bioinformatic observations (Figure 5(a)). The most intense areas of interaction between FapC protein and CsgA peptides are in the R1 and R3 regions, suggesting that these APR regions are not only important for inter- or intra molecular CsgA-CsgA interactions but also play a central role in the interaction between CsgA peptides and FapC protein. The one clear area in the CsgA peptide array without overlapping interaction profiles between CsgA and FapC is in the R5 region. The R5 repeat distinguishes itself from the remaining repeats in totally lacking charged residues. If electrostatic interactions are important for the interaction between FapC protein and CsgA peptides, this will obviously reduce the level of contact in the R5 region.

Having demonstrated interaction between FapC protein and CsgA peptides, we performed the complementary analysis of exposing full-length CsgA to FapC peptides, using a peptide array containing the entire FapC sequence displayed as 14-mers peptides. Also in this experiment, we observed substantial segments of shared binding areas of FapC and CsgA (Figure S15), supporting our previous observations of potential cross-interactions between segments of CsgA and FapC. The most pronounced areas of interactions between CsgA protein and FapC peptides contained positively charged lysine residues,

supporting a possible role of electrostatic interactions between CsgA and FapC.

CsgA-derived peptides inhibit both E. Coli and P. Aeruginosa biofilms, suggesting a broad-spectrum effect

Having demonstrated that many of our peptides modulate CsgA and FapC fibrillation *in vitro*, we next investigated their effect on functional bacterial amyloids in *E. coli* and *P. aeruginosa* biofilms. As a positive control for biofilm reduction, we used the small molecule epigallocatechin-3-gallate (EGCG), which has previously been shown to reduce biofilm formation of *E. coli* by reducing the expression of the CsgA-transcription activator, CsgD.[54] Further, EGCG has been shown to modulate the fibrillation of both PAO1 FapC[55] and UK4 FapC,[56] *in vitro*, in addition to remodeling FapC fibrils in mature *P. aeruginosa*[55] biofilms and reducing the biofilm formation in *Pseudomonas sp.* UK4.[56] The bacteria were co-incubated with 50 μg/mL peptides or EGCG during the biofilm attachment phase. This concentration was half of that used in our ThT-assay screens. After 24 h, the amount of biofilm was quantified using crystal violet staining. Several peptides significantly reduced the crystal violet staining of biofilm in *E. coli* cultures compared to untreated cultures, suggesting a reduction in biofilm formation (Fig. 6a and Figure S16(a)). The negative controls, P20 and P2, showed no effect as in our *in vitro* fibrillation experiments. These results indicated a peptide-induced modulation of curli fibrils, leading to a reduction of biofilm formation. Interestingly, analogous to our *in vitro* assays, the effect of the peptides was dependent on the number of Arg residues. Thus the only difference between the non-biofilm reducing P24 and the biofilm-reducing P25 was the number of Arg residues (4 in P24 vs. 6 in P25). The same applies to P27 (4) vs. P28 (6). These two peptides are identical except for the number of Arg residues but P28 reduces biofilm more dramatically than P27 (Figure S16 and Table S1). The apparent correlation between the number of Arg residues and biofilm reduction may be explained by the documented effect of positively charged residues on peptide uptake in bacteria,[57] which was also observed previously for the same peptide design strategy.[31]

Next, the effect of peptides was investigated in *P. aeruginosa* biofilms. Remarkably, several peptides also significantly reduced the crystal violet staining of biofilms in *P. aeruginosa*, which suggested that CsgA-derived peptides also modulated Fap fibrillation *in vivo* (Figure 6(b) and Figure S16(b)). The hexapeptide, P53 effectively reduced the crystal violet staining of biofilms both strains, suggesting a reduced formation of biofilm (Figure 6(a,b)) in accordance with the interaction of the peptide with both CsgA and FapC observed *in vitro.* Eight of our peptides (of which five were hexapeptides) caused a significant modulation of
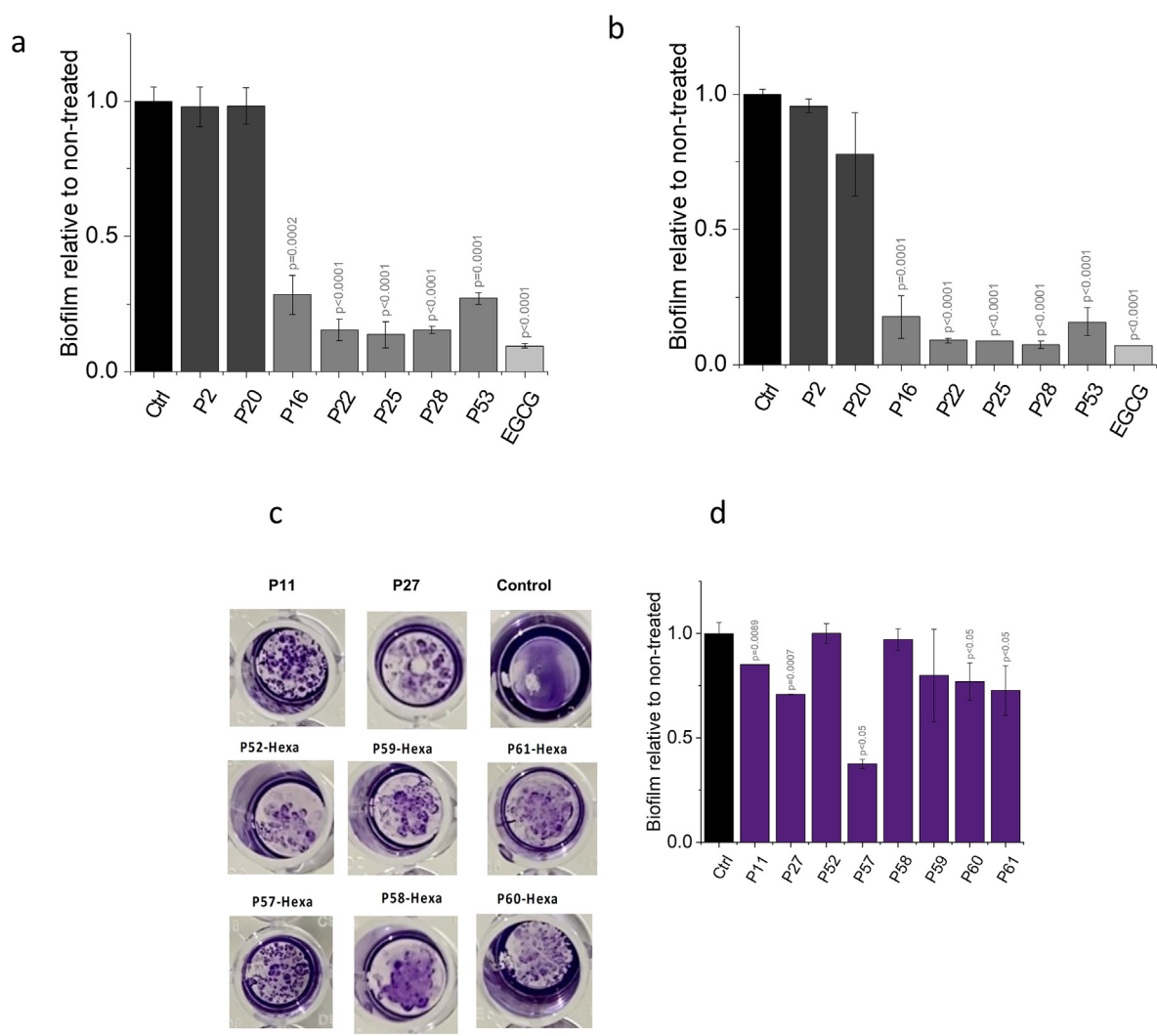
Figure 6. Peptide-induced reduction of bacterial biofilm formation measured using crystal violet. Biofilm formation in the absence and presence of selected peptides in (a) *Escherichia coli* and (b) *Pseudomonas aeruginosa.* (c) Changed morphology of *Escherichia coli* biofilms after treatment with CsgA-targeted peptides. (d) Biofilm formation in the absence and presence of peptides that change the morphology of *Escherichia coli.* Error bars are standard deviation (n = 3).

the morphology of *E. coli* biofilms (Figure 6(c)), altering it from a uniform lawn-like layer to more granulated structures. The changed morphology of the biofilms treated with fibrillating hexapeptide may be explained by a potential agglutination of the bacteria as observed previously in the presence of different fibrillating hexapeptides.[58] The biofilms with a changed morphology showed a modest reduction in crystal violet staining or no reduction (Figure 6(d)). It should be noted that the formation of agglutinated biofilms might result in reduced absorbance but not necessarily a reduction of the total amount of biofilm, and the results should therefore be interpreted with caution. The only biofilm-reducing hexapeptide, P53, stood out as the only hexapeptide to contain an Arg residue. This, again, supported the hypothesis that positively charged residues induce peptide uptake in bacteria,

which leads to effective biofilm-reduction by peptide-induced CsgA or FapC fibrillation modulation. To confirm that peptides are indeed taken up by bacteria, we turned to super-resolution Structured Illumination Microscopy (SIM). We treated bacteria with fluorescein-conjugated derivatives of P19, P53 and P35-R2 with an 6-aminohexanoic acid (Ahx) linker for 1 h at a final concentration of 50 μg/mL. Peptide internalization was verified by the formation of fluorescent peptide accumulations within bacteria at the poles (Figure 7(a)).

Peptide-induced diverted aggregation of CsgA is not toxic in mammalian cells

To test whether aggregates of CsgA formed in the presence of our biofilm-targeting peptides are toxic to eukaryotic cells, we exposed human embryonic
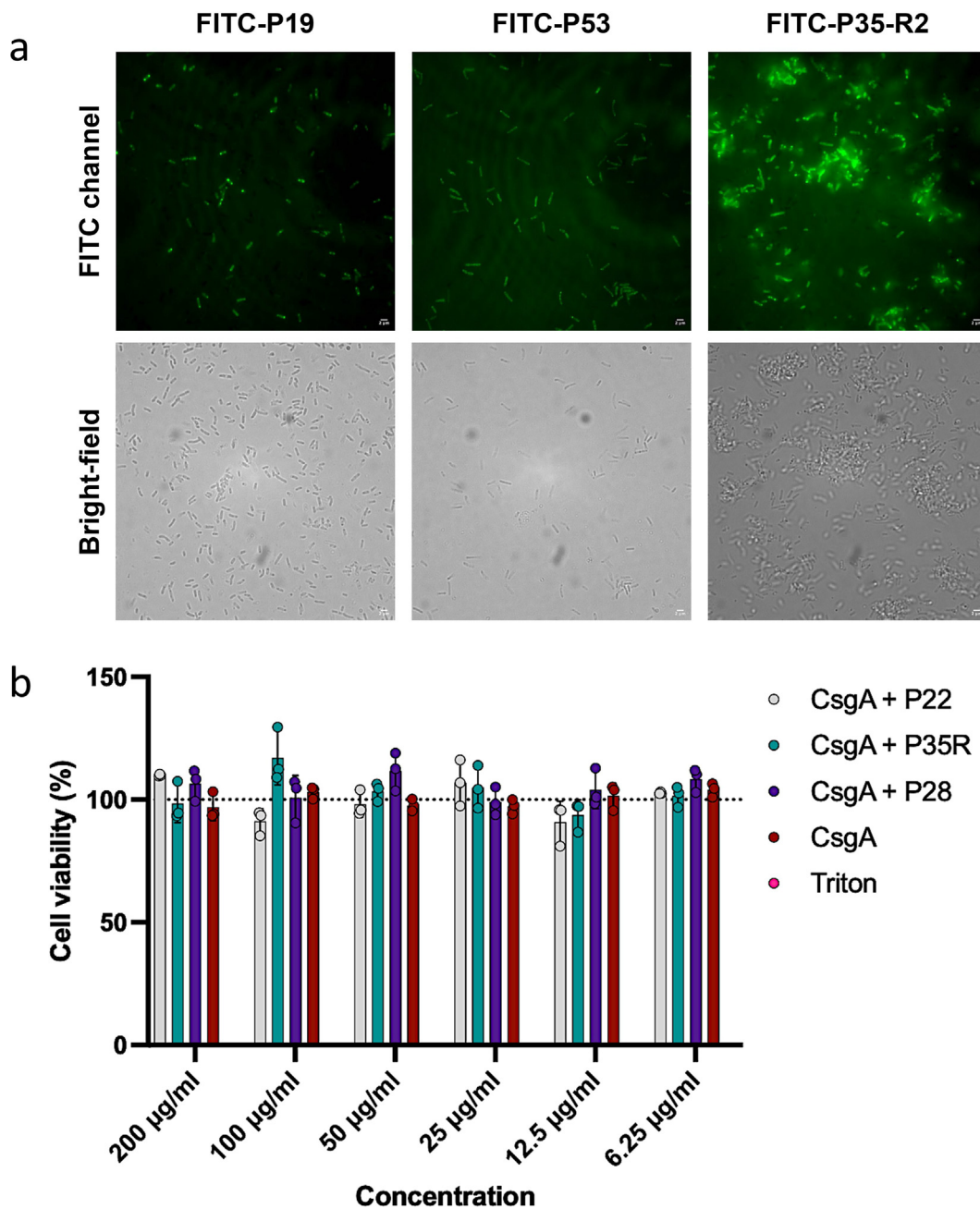
Figure 7. Peptide uptake into bacteria and eukaryotic cell viability assay. (a) Peptide uptake into bacteria. Top panel: Fluorescence detection of E. coli bacteria treated with FITC-derivatives of P19, P53 and P35-R2 using SIM. Bottom panel: Bright-field detection. Scale bar = 2 μm Aggregates prepared by incubation of CsgA mixed with peptides in a 1:1 analogy or by CsgA alone are not toxic to HEK293T cells. (b) Cell viability assay. HEK293T cells were incubated by a gradient of concentrations of aggregates of CsgA alone or aggregated with peptides in a 1:1 ratio.

kidney (HEK293T) cells to different concentrations of these aggregates for 24 h and measured cell viability using the CellTiter-blue assay. Gratifyingly, our results showed that neither the CsgA protein alone nor the CsgA aggregates formed in the presence of the peptides are toxic to HEK293T cells (Figure 7(b)).

Discussion

Peptides redirect functional bacterial amyloids into destabilized aggregates

Our study demonstrates that CsgA fibrillation can be modulated using peptides targeted against its APRs. Several peptides caused a rapid increase

in turbidity, altered fibril morphology and decreased aggregate stability against formic acid dissolution. Remarkably, multiple CsgA-targeted peptides also modulated fibrillation of the unrelated functional amyloid FapC, likely through interaction with FapC segments that share structural and partial sequence similarity with CsgA. Having demonstrated the modulation of the two biofilm-related amyloid components, *in vitro*, we next demonstrated that several of our peptides reduce biofilm formation in *E. coli* and *P. aeruginosa*, suggesting that the peptides also reduce bacterial amyloid formation *in vivo*. An important conclusion is that our peptides do not inhibit aggregation *per se*. Instead, they redirect CsgA into aggregates with a markedly different morphology and lower stability than non-treated curli fibrils. These modulated CsgA aggregates are likely to have lost many of their desirable functional properties. This was illustrated by aggregates formed in presence of e.g., peptide P11-r2, which were dominated by oligomer-like aggregates and only short crystalline fibrils, which were almost completely dissolved in our formic acid screen. In contrast, less than 20% of untreated CsgA was dissolved, reflecting the dramatic reduction in formic-acid stability upon treatment with peptides.

CsgA fibrillation may be blocked by peptide "cappers"

We speculate that our most effective peptides function as fibril-end "cappers", which associate with fibril ends and block further elongation of the fibril, forcing the aggregate to grow more irregularly, e.g. by lateral association of incoming monomeric CsgA. This was supported by our seeded CsgA fibrillation experiments, which showed a dramatic decrease in the slope of the fibrillation curve in the presence of peptides. Fibril end-blocking peptides should have a considerably higher affinity for the ends of CsgA fibril compared to monomeric CsgA.[32] We identified CsgA-interacting peptides in our SPR experiment, which perfectly matched the results from our fibrillation ThT experiment. That is, ThT-fluorescence reducing peptides also showed CsgA-binding in SPR, whereas peptides with no effect in ThT-assays showed no CsgA-binding in SPR-experiment. Despite this, the affinity between immobilized monomeric CsgA on the SPR chip and the interacting peptides was relatively low (i.e., μM range K_D) compared to the dramatic effect of the peptide-induced fibrillation modulation. However, if our peptides largely function as fibril-end "cappers" which recognize pre-formed β-sheet structures, a relatively low affinity between monomeric (and thus unfolded) CsgA and peptides is not surprising, since binding is likely to be coupled to induction of β-sheet structure.[32] In these coupled reactions, the work required to fold the CsgA target site will lead to a decrease in the overall (apparent) affinity for the

peptide. We did not investigate the affinity between peptides and fibril ends but this may be a potential future study to provide further insight into the inhibitory mechanism of the peptides. However, the strong peptide effect against seeded CsgA fibrillation suggests a fibril end-capping effect of our peptides. In a recent comprehensive *in silico* thermodynamic profiling of heterotypic interactions with fibril ends, we showed that fibril-end capping peptides were most efficiently obtained by introducing positively charged or aromatic residues.[32] This is in accordance with observations in our present study, where our most efficient peptides were those with the highest number of Arg and Trp residues.

Peptides may bind segments in FapC with structural and sequence similarity to CsgA

We also demonstrated modulation of FapC fibrillation using our CsgA-derived peptides, which is likely a result of sequence and structural similarity between the APRs of CsgA and FapC. Despite this, no effective cross-seeding was caused by CsgA seeds on FapC monomers. This suggests that only shorter CsgA sequences are able to interact with FapC. Interestingly, common modulators of CsgA and FapC have been described before. The CsgA chaperone, CsgC (which also inhibits aggregation of α-synuclein related to Parkinson's disease[16,55]) reduces both CsgA and FapC fibrillation *in vitro*.[17] A broad spectrum of other anti-amyloid chaperones such as DNAJB6, TTR, S100A9 and Bri2 also target both CsgA and FapC though to variable extents.[61] These chaperones show a diverse range of amyloid-inhibitory mechanisms, but the existence of shared fibrillation modulators between proteins with different sequences illustrates that structural similarity perhaps plays a bigger role than sequence similarity. Indeed, CsgA, FapC, and even α-synuclein share some structural similarities, given that they all contain a cross-β spine. CsgA also shares common peptide inhibitors with Alzheimer's disease-associated amyloid-β, an observation that the authors attribute to structural similarity between CsgA amyloid-β.[38] These examples serve to show that for some amyloid modulating molecules, the primary sequence of target amyloids may only play a secondary role, possibly because the main stabilizing forces of the cross-β spine are hydrogen bonds between backbone atoms and not between side chains.[1,2] However, the primary sequences of amyloids do play an important role and even single-residue substitutions can influence a protein's ability to form amyloid[62–65] or peptide modulators' ability to seed heterogeneous aggregation.[35] A low tolerance of sequence mismatch is probably most significant in amyloids consisting of homo-steric zippers, i.e., amyloids where sidechains tightly associate with sidechains of the same kind.[65] There may be situations where a larger mismatch may be tolerated. Supporting this line of thought,

CsgA and FapC are perfect examples of amyloids that tolerate a certain degree sequence mismatch between their β-strands. Structure predictions of both proteins show hetero-steric zippers,[21,61] meaning that the sidechains are associated with sidechains of unequal sequence in all β-strands. Hetero-steric zippers are not a unique feature of FuBA since they also exist in many pathological amyloids.[67] However, in FuBA, not only are there sequence mismatches in their steric zippers but also within the stacked β-strands, and FuBA sequences are described as containing "imperfect repeats".[6,7] This tolerance of mismatches in FuBA may help to explain why a considerable number of our peptides interacted with both CsgA and FapC.

Rapid precipitation of target protein may work better than delaying fibrillation

The success criteria of many previously described amyloids inhibitors have often been whether they delay the onset of fibrillation.[68–70] While this may be a useful strategy in relation to pathological amyloids, it may not be the best way to target bacterial amyloids. In bacterial communities, inhibitors may over time be degraded or the bacteria learn to cope with the drugs, e.g., by finding ways to export them.[71,67] Several of our peptides appear to cause a prompt precipitation of CsgA, essentially removing CsgA from the solution before proper fibrillation can take place. We argue that this strategy, under certain circumstances, can be better than simply delaying the onset of fibrillation. In support of this, we observed peptides that caused a rapid CsgA precipitation were more consistent in reducing the stability of CsgA aggregates, as observed by formic acid solubility, compared to peptides which delayed CsgA fibrillation (i.e., caused longer fibrillation half-times).

Peptide-induced reduction of biofilm formation could be a result of intracellular modulation of CsgA and FapC

Peptide incubation of *E. coli* and *P. aeruginosa* cultures led to a reduction in biofilm formation which may be explained by the modulation of CsgA and FapC fibrillation *in vivo*. Positively charged residues appeared to increase the effect of the peptides. Positively charged residues are known to increase peptide uptake in bacteria[57] and indeed we see significant uptake of peptides into the bacterial cytosol. This suggests that the most effective reduction in biofilm formation is obtained by intracellularly modulating CsgA and FapC fibrillation. This is interesting, considering that both CsgA and FapC are transported to the cell surface during curli or Fap biogenesis, and they could potentially be modulated by peptides after reaching the cell surface in peptide-treated bacterial cultures. However, CsgA and FapC are expected to be nucleated by CsgB and FapB, respectively, on the cell surface. *In vitro*, CsgA nucleation by CsgB is immediate and happens without a lag phase.[73] Such an effective nucleation would likely mitigate the effect of modulating peptides. In light of this, it would make sense that the two proteins are more prone to peptide-induced modulation intracellularly, before making contact with their nucleator proteins on the cell surface.

Structure-based design of fibrillation modulators is a promising approach to inhibit biofilm formation

In conclusion, *in silico* amyloid-predictors have existed for almost two decades and have been largely accurate in predictions of "canonical" APRs with high hydrophobicity and β-sheet propensity.[30] The recent development of *in silico* amyloid predictors[29] has improved the accuracy of predictions of less "canonical" (e.g., more hydrophilic and charged) APRs in bacterial amyloids. In addition, *in silico* thermodynamic profiling of APRs has improved the structure-based design of fibrillation-modulating peptides.[32] Here we have exploited these approaches to modulate the fibrillation of bacterial amyloids from *E. coli* and *Pseudomonas*. We extended our findings to inhibit the biofilm formation in *E. coli* and the clinically important pathogen, *P. aeruginosa*. Combined with our observation that the "diverted" CsgA-peptide aggregates are not toxic to human cells, we expect that these findings will have important consequences in the further development of anti-biofilm therapeutics.

Materials and Methods

Expression and purification of CsgA and FapC protein

Recombinant CsgA and FapC proteins were expressed and purified as described.[23,69] Peptides were purchased from Genscript (Piscataway, NJ) with a purity of >98%. Peptide arrays were produced as described.[50]

Computational analysis of CsgA

Computational prediction of APR regions in CsgA using Cordax, Waltz and Tango was performed as described previously.[29] Aggregation propensity was also predicted using Aggrescan,[76] Metamyl,[77] MILAMP[78] and PASTA 2.0.[79] The aggregation propensity score from all predictors was normalized. The individual normalized values from Cordax, Waltz and Tango were plotted. For comparison, an average score was calculated from Aggrescan, Metamyl, MILAMP, PASTA 2.0 Waltz and Tango. Structural models of the CsgA segments $_{43}$SELNIY$_{48}$ and $_{55}$SALALQ$_{60}$ were produced using Cordax as described previously.[29] Peptides for strategy 3 were designed based on thermodynamic calculations using the Cordax-derived template

structures and the FoldX force field[45] as described previously.[32]

Fibrillation assay of CsgA and FapC in the presence of CsgA-targeted peptides

CsgA or FapC in elution buffer (8 M GdmCl, 50 mM Tris-HCl, 500 mM imidazole, pH 8) was buffer exchanged into 50 mM Tris-HCl, pH 7.4 using PD-10 desalting columns (GE Healthcare Life Sciences, Brøndby, Denmark) according to manufacturer's protocol. CsgA or FapC protein concentration was estimated by measuring the absorbance at 280 nm (extinction coefficients and molecular weights shown in supplementary appendix 1) using a NanoDrop 1000 (ND-1000 Spectrophotometer, Scientific, Waltham, MA). Final protein concentrations were adjusted to 0.1 mg/mL. Peptides (20 mg/mL in 100% Dimethyl sulfoxide (DMSO) were added to a final concentration of 0.1 mg/mL, obtaining a CsgA: Peptide mass ratio of 1:1. ThT was added to a final concentration of 20 μM. The peptide concentration in dose response experiments is shown in relevant figures. Samples with a volume of 200 μL were added to a 96 well plate (Costar, Corning) in duplicates and the plate was sealed with clear plastic film. The plate was inserted into a Clariostar plus plate reader (BMG Labtech, Ortenberg, Germany) and the experiment was carried out using the following settings: Measurement of ThT fluorescence by excitation at 448.2 nm and emission at 485 nm by bottom reads, gain: 1500, temperature: 37 °C. Measurements were taken every 10 min and orbital shaking at 100 rpm was applied for 2 sec between reads. After the end of fibrillation, 50 μL of each was centrifuged at 13,500 rpm for 10 min and the supernatant was examined for remaining soluble CsgA protein by SDS-PAGE analysis. Fibrillation half-times ($t_{1/2}$) were determined using the AmyloFit half-time calculator.[80] Turbidity measurements performed on a Varioskan Flash plate reader (Thermo Scientific, Waltham, MA) at 600 nm using a bandwidth of 5 nm and 1 s integration time. Seeded fibrillation assays were performed as explained above with the exception that 96-well plates with non-binding surface were used (Costar, Corning). Solutions with 0.09 mg/mL preformed fibrils were sonicated for 30 s before they diluted into monomer solutions to a final seed concentration of 0.5 mg/mL (5% w/w). P values were calculated using a two-tailed, equal variance *t* test.

Surface Plasmon Resonance (SPR)

SPR experiments were carried out at 25 °C using a Biacore 3000 system. CsgA monomers (0.7 mg/mL) were immobilized on a Carboxymethylated CM5 chip activated by 50 mM 1-ethyl-3-(3-dimethy

laminopropyl)-carbodiimide and 200 mM N-hydroxy succinimide. An immobilization level of 5000 response units was achieved. Peptides (20 mg/mL in DMSO) were diluted to the required concentrations (5–200 μM) in 10 mM HEPES, 150 mM NaCl, pH 7.4 and injected over the immobilized CsgA monomers at a flow rate of 20 μL/min for 150 s. After saturation of the peptide binding on CsgA, the dissociation was monitored for 500 s.

TEM analysis of CsgA aggregates formed in the presence of peptides

Transmission electron microscopy (TEM) images were taken of the samples at the endpoint of the ThT assays using the following procedure: $\sim$10 μL of sample was placed on top of a glow discharged carbon coated nickel grid. The grid was washed with distilled water and stained with 2% (w/v) aqueous uranyl acetate. The grid was dried for excess stain with filter paper imaged with a Tecnai G2 spirit transmission electron microscope.

Formic acid stability measurement of CsgA aggregates formed in the presence of peptides

The stability towards formic acid of CsgA aggregates formed in the presence of peptides was measured by the following procedure: CsgA aggregates were pelleted by centrifugation at 13,500 rpm for 15 min. The supernatant was examined for remaining monomeric CsgA by absorbance measurement at 280 nm (ND-1000 Spectrophotometer, Scientific, Waltham, MA).

The supernatant was discarded, and the fibrils were resuspended in 50% and 100% formic acid in MQ water to a final protein concentration of 0.5 mg/mL. The fibrils were incubated in the formic acid solution for 10 min at RT and then centrifuged at 13,500 rpm for 15 min. A volume of 20 μL of the supernatant from each sample was transferred to new Eppendorf tubes. The samples were frozen in liquid nitrogen and lyophilized for 8 h, followed by resuspension in 20 μL SDS-PAGE sample buffer prior to SDS-PAGE on a 15% poly-acrylamide Bis-Tris gel. To determine percentage of solubilized CsgA, the band intensities were quantified using ImageJ and normalized relative to control samples. P values were calculated using a two-tailed, equal variance *t* test.

Biofilm assays

The biofilm formation of peptide-treated *E. coli Keio* and *P. aeruginosa* was quantified using crystal violet staining using a similar procedure as described previously.[81] Overnight cultures of *E. coli Keio* and *P. aeruginosa* were diluted to an OD_{600} of 0.005 and a volume of 200 μL was added

to the wells of a 96-well microtiter plate. Peptides were added to a final concentration of 50 μg/mL. Control samples containing EGCG at a final concentration of 50 μg/mL were also prepared. The 96-well microtiter plate was then incubated at 37 °C for 24 h. Following incubation, remaining planktonic bacteria were removed and the wells were rinsed three times with phosphate-buffered saline (PBS) and dried for 1 h at r.t. The dried biofilms were stained with 200 μl 1% (w/v) crystal violet (Sigma) for 10 min. This was followed by three times wash with water and drying. The stain biofilms were released using 200 μl of 30% (v/v) acetic acid solution and quantified by measuring the absorbance of crystal violet at 585 nm in a UV/VIS plate reader. The biofilm formation of each culture was normalized relative to negative control samples. P values were calculated using a two-tailed, equal variance t test.

Super-resolution microscopy of peptide-treated bacteria

Exponentially growing E. coli Keio bacteria were washed twice with sterile physiological water and diluted to 0.5 McFarland standard (1.5×10^8 CFU/mL). 1 mL bacterial suspension was treated with FITC-labelled peptides (final concentration 50 μg/mL) for 1 h at 37 °C. Then the bacteria were washed and imaged with a Zeiss Elyra S.1 super-resolution microscope using filters for FITC (excitation 450 nm, emission 520/20 nm). The acquired images were analysed using the image processing software Fiji.[82]

Cell toxicity assays with CsgA aggregates

Peptides P22, P35R and P28 (20 mg/mL in 100% DMSO were each mixed with CsgA to a final concentration of 0.3 mg/mL of both peptide and protein, obtaining a CsgA:peptide mass ratio of 1:1 and incubated while shaking for 24 h at 37 °C as for the preceding fibrillation assays (see above). Suspension of these aggregates were subsequently incubated with HEK293 cells as follows: HEK 293 T human embryonic kidney cells (6×10^4 per well) were seeded in 96-well flat bottom plates in Dulbecco's modified Eagle's medium, and incubated with different concentrations of peptides for 24 h. The viability of the cells at the end of the incubation was determined by the intracellular reduction of resazurin into resorufin using CellTiter-Blue kit. CellTiter-Blue reagent (40 μl per well) was added in the 96-well plate, followed by orbital shaking at 100 rpm for 10 s. The plate was then incubated in a CO_2 incubator for 4 h, followed by reading the fluorescence signal (excitation 544 nm, emission 590 nm). Cells treated with 1% Triton X-100 and vehicle were considered positive and negative controls, respectively.

DATA AVAILABILITY

Data will be made available on request.

Declaration of Competing Interest

The authors declare that they have no known competing financial interests or personal relationships that could have appeared to influence the work reported in this paper.

Appendix A. Supplementary data

Supplementary data to this article can be found online at https://doi.org/10.1016/j.jmb.2023.168039.

References

1. Chiti, F., Dobson, C.M., (2017). Protein Misfolding, Amyloid Formation, and Human Disease: A Summary of Progress Over the Last Decade. *Annu. Rev. Biochem* **86**, 27–68. https://doi.org/10.1146/annurev-biochem-061516-045115.

2. Jahn, T.R., Makin, O.S., Morris, K.L., Marshall, K.E., Tian, P., Sikorski, P., Serpell, L.C., (2010). The Common Architecture of Cross-β Amyloid. *J. Mol. Biol.* **395**, 717–727. https://doi.org/10.1016/j.jmb.2009.09.039.

3. Riek, R., Eisenberg, D.S., (2016). The activities of amyloids from a structural perspective. *Nature* **539**, 227–235. https://doi.org/10.1038/nature20416.

4. Fink, A.L., (2006). in *Misbehaving Proteins* 265–285. Springer.

5. Chiti, F., Dobson, C.M., (2006). Protein Misfolding, Functional Amyloid, and Human Disease. *Annu. Rev. Biochem* **75**, 333–366. https://doi.org/10.1146/annurev.biochem.75.101304.123901.

6. Chapman, M.R., Robinson, L.S., Pinkner, J.S., Roth, R., Heuser, J., Hammar, M., Normark, S., Hultgren, S.J., (2002). *Role of Escherichia coli curli operons in directing amyloid fiber formation. Science* **295**, 851–855.

7. Dueholm, M.S., Petersen, S.V., Sønderkær, M., Larsen, P., Christiansen, G., Hein, K.L., Enghild, J.J., Nielsen, J.L., et al., (2010). Functional amyloid in pseudomonas. *Mol. Microbiol.* **77**, 1009–1020. https://doi.org/10.1111/j.1365-2958.2010.07269.x.

8. Dueholm, M.S., Nielsen, P.H., Chapman, M., Otzen, D., Romero, D., Kolter, R., Dueholm, M.S., Nielsen, P.H., et al., (2013). 411–438. Wiley-VCH Verlag GmbH & Co, KGaA.

9. Zeng, G., Vad, B.S., Dueholm, M.S., Christiansen, G., Nilsson, M., Tolker-Nielsen, T., Nielsen, P.H., Meyer, R.L., et al., (2015). Functional bacterial amyloid increases Pseudomonas biofilm hydrophobicity and stiffness. *Front. Microbiol.* **6**, 1–14. https://doi.org/10.3389/fmicb.2015.01099.

10. Wang, X., Smith, D.R., Jones, J.W., Chapman, M.R., (2007). In vitro polymerization of a functional Escherichia coli amyloid protein. *J. Biol. Chem.* **282**, 3713–3719. https://doi.org/10.1074/jbc.M609228200.

11. Dueholm, M.S., Nielsen, S.B., Hein, K.L., Nissen, P., Chapman, M., Christiansen, G., Nielsen, P.H., Otzen, D.E., (2011). Fibrillation of the major curli subunit CsgA under a wide range of conditions implies a robust design of aggregation. *Biochemistry* **50**, 8281–8290. https://doi.org/10.1021/bi200967c.

12. Hammar, M., Arnqvist, A., Bian, Z., Olsén, A., Normark, S., (1995). Expression of two csg operons is required for production of fibronectin- and Congo red-binding curli polymers in Escherichia coli K-12. *Mol. Microbiol.* **18**, 661–670. https://doi.org/10.1111/j.1365-2958.1995.mmi_18040661.x.

13. White, A.P., Collinson, S.K., Banser, P.A., Gibson, D.L., Paetzel, M., Strynadka, N.C.J., Kay, W.W., (2001). Structure and characterization of AgfB from Salmonella enteritidis thin aggregative fimbriae. *J. Mol. Biol.* **311**, 735–749. https://doi.org/10.1006/jmbi.2001.4876.

14. Nenninger, A.A., Robinson, L.S., Hultgren, S.J., (2009). Localized and efficient curli nucleation requires the chaperone-like amyloid assembly protein CsgF. *Proc. Natl. Acad. Sci.* **106**, 900–905. https://doi.org/10.1073/pnas.0812143106.

15. Evans, M.L. et al, (2015). *The Bacterial Curli System Possesses a Potent and Selective Inhibitor of Amyloid Formation Article The Bacterial Curli System Possesses a Potent and Selective Inhibitor of Amyloid Formation.* **445–455** https://doi.org/10.1016/j.molcel.2014.12.025.

16. Taylor, J.D. et al, (2016). Electrostatically-guided inhibition of Curli amyloid nucleation by the CsgC-like family of chaperones. *Nature Publ. Group* **1–11** https://doi.org/10.1038/srep24656.

17. Robinson, L.S., Ashman, E.M., Hultgren, S.J., Chapman, M.R., (2006). *Secretion of curli fibre subunits is mediated by the outer membrane-localized CsgG protein.* **59**, 870–881. https://doi.org/10.1111/j.1365-2958.2005.04997.x.

18. Hammer, N.D., Schmidt, J.C., Chapman, M.R., (2007). The curli nucleator protein, CsgB, contains an amyloidogenic domain that directs CsgA polymerization. *PNAS* **104**, 12494–12499. https://doi.org/10.1073/pnas.0703310104.

19. Barnhart, M.M., Chapman, M.R., (2006). Curli biogenesis and function. *Annu. Rev. Microbiol.* **60**, 131–147. https://doi.org/10.1146/annurev.micro.60.080805.142106.

20. Tian, P., Boomsma, W., Wang, Y., Otzen, D.E., Jensen, M.H., Lindorff-Larsen, K., Lindor, K., (2015). Structure of a Functional Amyloid Protein Subunit Computed Using Sequence Variation. *J. Am. Chem. Soc.* **19–22** https://doi.org/10.1021/ja5093634.

21. Collinson, S.K., Parker, J.M.R., Hodges, R.S., Kay, W.W., (1999). Structural predictions of AgfA, the insoluble fimbrial subunit of Salmonella thin aggregative fimbriae. *J. Mol. Biol.* **290**, 741–756. https://doi.org/10.1006/jmbi.1999.2882.

22. Sonderby, T.V., Rasmussen, H.O., Frank, S.A., Skov Pedersen, J., Otzen, D.E., (2021). Folding Steps in the Fibrillation of Functional Amyloid: Denaturant Sensitivity

Reveals Common Features in Nucleation and Elongation. *J. Mol. Biol.* **434**, https://doi.org/10.1016/j.jmb.2021.167337 167337.

23. Wang, X., Zhou, Y., Ren, J.-J., Hammer, N.D., Chapman, M.R., (2010). *Gatekeeper residues in the major curlin subunit modulate bacterial amyloid fiber biogenesis.* **107**, 163–168. https://doi.org/10.1073/pnas.0908714107.

24. Olsen, A., Jonsson, A., Normark, S., (1989). Fibronectin binding mediated by a novel class of surface organelles on Escherichia coli. *Nature* **338**, 652–655. https://doi.org/10.1038/338652a0.

25. Herwald, H., Mörgelin, M., Olsén, A., Rhen, M., Dahlbäck, B., Müller-Esterl, W., Björck, L., (1998). Activation of the contact-phase system on bacterial surfaces—a clue to serious complications in infectious diseases. *Nature Med.* **4**, 298–302.

26. de la Paz, M.L., Serrano, L., (2004). Sequence determinants of amyloid fibril formation. *Proc. Natl. Acad. Sci.* **101**, 87–92.

27. Fernandez-Escamilla, A.M., Rousseau, F., Schymkowitz, J., Serrano, L., (2004). Prediction of sequence-dependent and mutational effects on the aggregation of peptides and proteins. *Nature Biotechnol.* **22**, 1302–1306. https://doi.org/10.1038/nbt1012.

28. Louros, N., Orlando, G., De Vleeschouwer, M., Rousseau, F., Schymkowitz, J., (2020). Structure-based machine-guided mapping of amyloid sequence space reveals uncharted sequence clusters with higher solubilities. *Nature Commun.* **11**, 1–13.

29. Trainor, K., Broom, A., Meiering, E.M., (2017). Exploring the relationships between protein sequence, structure and solubility. *Curr. Opin. Struct. Biol.* **42**, 136–146. https://doi.org/10.1016/j.sbi.2017.01.004.

30. Khodaparast, L. et al, (2018). Aggregating sequences that occur in many proteins constitute weak spots of bacterial proteostasis. *Nature Commun.* **9** https://doi.org/10.1038/s41467-018-03131-0.

31. Louros, N., Ramakers, M., Michiels, E., Konstantoulea, K., Morelli, C., Garcia, T., Moonen, N., D'Haeyer, S., et al., (2022). Mapping the sequence specificity of heterotypic amyloid interactions enables the identification of aggregation modifiers. *Nature Commun.* **13**, 1–20.

32. Betti, C., Vanhoutte, I., Coutuer, S., De Rycke, R., Mishev, K., Vuylsteke, M., Aesaert, S., Rombaut, D., et al., (2016). Sequence-specific protein aggregation generates defined protein knockdowns in plants. *Plant Physiol.* **171**, 773–787.

33. Gallardo, R., Ramakers, M., De Smet, F., Claes, F., Khodaparast, L., Khodaparast, L., Couceiro, J.R., Langenberg, T., et al., (2016). De novo design of a biologically active amyloid. *Science* **354**, aah4949.

34. Khodaparast, L., Wu, G., Khodaparast, L., Schmidt, B.Z., Rousseau, F., Schymkowitz, J., (2021). Bacterial Protein Homeostasis Disruption as a Therapeutic Intervention. *Front. Mol. Biosci.* **8**, 681855. https://doi.org/10.3389/fmolb.2021.681855.

35. Wu, G., Khodaparast, L., Khodaparast, L., De Vleeschouwer, M., Housmans, J., Houben, B., Schymkowitz, J., Rousseau, F., (2021). Investigating the mechanism of action of aggregation-inducing antimicrobial Pept-ins. *Cell Chem. Biol.* **28**, 524–536.e524. https://doi.org/10.1016/j.chembiol.2020.12.008.

36. Louros, N., Konstantoulea, K., De Vleeschouwer, M., Ramakers, M., Schymkowitz, J., Rousseau, F., (2020). WALTZ-DB 2.0: an updated database containing structural information of experimentally determined amyloid-forming peptides. *Nucleic Acids Res.* **48**, D389–D393. https://doi.org/10.1093/nar/gkz758.

37. Perov, S., Lidor, O., Salinas, N., Golan, N., Tayeb-Fligelman, E., Deshmukh, M., Willbold, D., Landau, M., (2019). Structural Insights into Curli CsgA Cross-beta Fibril Architecture Inspire Repurposing of Anti-amyloid Compounds as Anti-biofilm Agents. *PLoS Pathog.* **15**, e1007978.

38. Dunbar, M., DeBenedictis, E., Keten, S., (2019). Dimerization energetics of curli fiber subunits CsgA and CsgB. *npj Comput. Mater.* **5**, 27. https://doi.org/10.1038/s41524-019-0164-5.

39. Louros, N.N., Bolas, G.M.P., Tsiolaki, P.L., Hamodrakas, S.J., Iconomidou, V.A., (2016). Intrinsic aggregation propensity of the CsgB nucleator protein is crucial for curli fiber formation. *J. Struct. Biol.* **195**, 179–189. https://doi.org/10.1016/j.jsb.2016.05.012.

40. Sleutel, M., Pradhan, B., Remaut, H., (2022). Structural analysis of the bacterial amyloid curli 2022.2002.2028.482343 *bioRxiv*. https://doi.org/10.1101/2022.02.28.482343.

41. Michiels, E. et al, (2020). Reverse engineering synthetic antiviral amyloids. *Nature Commun.* **11**, 2832. https://doi.org/10.1038/s41467-020-16721-8.

42. Schymkowitz, J., Borg, J., Stricher, F., Nys, R., Rousseau, F., Serrano, L., (2005). The FoldX web server: an online force field. *Nucleic Acids Res.* **33**, W382–W388. https://doi.org/10.1093/nar/gki387.

43. Robinson, L.S., Ashman, E.M., Hultgren, S.J., Chapman, M.R., (2006). Secretion of curli fibre subunits is mediated by the outer membrane-localized CsgG protein. *Mol. Microbiol.* **59**, 870–881.

44. Kajava, A.V., Steven, A.C., (2006). Beta-rolls, beta-helices, and other beta-solenoid proteins. *Adv. Protein Chem.* **73**, 55–96. https://doi.org/10.1016/S0065-3233(06)73003-0.

45. Richardson, J.S., Richardson, D.C., (2002). Natural beta-sheet proteins use negative design to avoid edge-to-edge aggregation. *PNAS* **99**, 2754–2759. https://doi.org/10.1073/pnas.052706099.

46. Christensen, L.F.B., Nowak, J.S., Sønderby, T.V., Frank, S.A., Otzen, D.E., (2020). Quantitating denaturation by formic acid: imperfect repeats are essential to the stability of the functional amyloid protein FapC. *J. Biol. Chem.* **295**, 13031–13046. https://doi.org/10.1074/jbc.RA120.013396.

47. Bleem, A., Christiansen, G., Madsen, D.J., Maric, H., Strømgaard, K., Bryers, J.D., Daggett, V., Meyer, R.L., et al., (2018). Protein Engineering Reveals Mechanisms of Functional Amyloid Formation in Pseudomonas aeruginosa Biofilms. *J. Mol. Biol.* **430**, 3751–3763. https://doi.org/10.1016/j.jmb.2018.06.043.

48. Jumper, J., Evans, R., Pritzel, A., Green, T., Figurnov, M., Ronneberger, O., Tunyasuvunakool, K., Bates, R., et al., (2021). Highly accurate protein structure prediction with AlphaFold. *Nature* **596**, 583–589.

49. Varadi, M., Anyango, S., Deshpande, M., Nair, S., Natassia, C., Yordanova, G., Yuan, D., Stroe, O., et al., (2022). AlphaFold Protein Structure Database: Massively expanding the structural coverage of protein-sequence space with high-accuracy models. *Nucleic Acids Res.* **50**, D439–D444.

50. Serra, D.O., Mika, F., Richter, A.M., Hengge, R., (2016). The green tea polyphenol EGCG inhibits E. coli biofilm formation by impairing amyloid curli fibre assembly and

downregulating the biofilm regulator CsgD via the σE-dependent sRNA RybB. *Mol. Microbiol.* **101**, 136–151.

51. Stenvang, M., Dueholm, M.S., Vad, B.S., Seviour, T., Zeng, G., Geifman-Shochat, S., Søndergaard, M.T., Christiansen, G., et al., (2016). Epigallocatechin gallate remodels overexpressed functional amyloids in pseudomonas aeruginosa and increases biofilm susceptibility to antibiotic treatment. *J. Biol. Chem.* **291**, 26540–26553. https://doi.org/10.1074/jbc.M116.739953.

52. Najarzadeh, Z., Mohammad-Beigi, H., Nedergaard Pedersen, J., Christiansen, G., Sønderby, T.V., Shojaosadati, S.A., Morshedi, D., Strømgaard, K., et al., (2019). Plant Polyphenols Inhibit Functional Amyloid and Biofilm Formation in Pseudomonas Strains by Directing Monomers to Off-Pathway Oligomers. *Biomolecules* **9**, 659.

53. Hancock, R.E., Chapple, D.S., (1999). Peptide antibiotics. *Antimicrob. Agents Chemother.* **43**, 1317–1323.

54. Chen, D., Li, J., Pan, T., Wu, R., Tao, Y., Lin, H., (2021). The broad-spectrum antibiofilm activity of amyloid-forming hexapeptides. *J. Microbial. Biotechnol.* **14**, 656–667.

55. Chorell, E., Andersson, E., Evans, M.L., Jain, N., Götheson, A., Åden, J., Chapman, M.R., Almqvist, F., et al., (2015). Bacterial Chaperones CsgE and CsgC Differentially Modulate Human α-Synuclein Amyloid Formation via Transient Contacts. *PLoS One* **10**, e0140194.

56. Nagaraj, M., Najarzadeh, Z., Pansieri, J., Biverstål, H., Musteikyte, G., Smirnovas, V., Matthews, S., Emanuelsson, C., et al., (2022). Chaperones mainly suppress primary nucleation during formation of functional amyloid required for bacterial biofilm formation. *Chem. Sci.* **13**, 536–553. https://doi.org/10.1039/D1SC05790A.

57. Liberta, F., Loerch, S., Rennegarbe, M., Schierhorn, A., Westermark, P., Westermark, G.T., Hazenberg, B.P.C., Grigorieff, N., et al., (2019). Cryo-EM fibril structures from systemic AA amyloidosis reveal the species complementarity of pathological amyloids. *Nature Commun.* **10**, 1104. https://doi.org/10.1038/s41467-019-09033-z.

58. Schütz, A.K., Vagt, T., Huber, M., Ovchinnikova, O.Y., Cadalbert, R., Wall, J., Güntert, P., Böckmann, A., et al., (2015). Atomic-resolution three-dimensional structure of amyloid β fibrils bearing the Osaka mutation. *Angew. Chem. Int. Ed.* **54**, 331–335.

59. Deng, X., Gonzalez Llamazares, A., Wagstaff, J.M., Hale, V.L., Cannone, G., McLaughlin, S.H., Kureisaite-Ciziene, D., Löwe, J., (2019). The structure of bactofilin filaments reveals their mode of membrane binding and lack of polarity. *Nature. Microbiology* **4**, 2357–2368. https://doi.org/10.1038/s41564-019-0544-0.

60. Sawaya, M.R., Sambashivan, S., Nelson, R., Ivanova, M.I., Sievers, S.A., Apostol, M.I., Thompson, M.J., Balbirnie, M., et al., (2007). Atomic structures of amyloid cross-β spines reveal varied steric zippers. *Nature* **447**, 453–457. https://doi.org/10.1038/nature05695.

61. Rouse, S.L., Matthews, S.J., Dueholm, M.S., (2018). Ecology and Biogenesis of Functional Amyloids in Pseudomonas. *J. Mol. Biol.* **430**, 3685–3695. https://doi.org/10.1016/j.jmb.2018.05.004.

62. Eisenberg, D., Jucker, M., (2012). The Amyloid State of Proteins in Human Diseases. *Cell* **148**, 1188–1203. https://doi.org/10.1016/j.cell.2012.02.022.

63. Willander, H., Presto, J., Askarieh, G., Biverstål, H., Frohm, B., Knight, S.D., Johansson, J., Linse, S., (2012). BRICHOS Domains Efficiently Delay Fibrillation of Amyloid β-Peptide*. *J. Biol. Chem.* **287**, 31608–31617. https://doi.org/10.1074/jbc.M112.393157.

64. Assarsson, A., Hellstrand, E., Cabaleiro-Lago, C., Linse, S., (2014). Charge Dependent Retardation of Amyloid β Aggregation by Hydrophilic Proteins. *ACS Chem. Nerosci.* **5**, 266–274. https://doi.org/10.1021/cn400124r.

65. Stanyon, H.F., Viles, J.H., (2012). Human Serum Albumin Can Regulate Amyloid-β Peptide Fiber Growth in the Brain Interstitium: IMPLICATIONS FOR ALZHEIMER DISEASE*. *J. Biol. Chem.* **287**, 28163–28168. https://doi.org/10.1074/jbc.C112.360800.

66. Blair, J.M., Richmond, G.E., Piddock, L.J., (2014). Multidrug efflux pumps in Gram-negative bacteria and their role in antibiotic resistance. *Future Microbiol.* **9**, 1165–1177.

67. Blair, J.M.A., Webber, M.A., Baylay, A.J., Ogbolu, D.O., Piddock, L.J.V., (2015). Molecular mechanisms of antibiotic resistance. *Nature Rev. Microbiol.* **13**, 42–51. https://doi.org/10.1038/nrmicro3380.

68. Swasthi, H.M., Mukhopadhyay, S., (2017). Electrostatic lipid–protein interactions sequester the curli amyloid fold on the lipopolysaccharide membrane surface. *J. Biol. Chem.* **292**, 19861–19872. https://doi.org/10.1074/jbc.M117.815522.

69. Rasmussen, C.B., Christiansen, G., Vad, B.S., Lynggaard, C., Enghild, J.J., Andreasen, M., Otzen, D., (2019). Imperfect repeats in the functional amyloid protein FapC reduce the tendency to fragment during fibrillation. *Protein Sci.* **28**, 633–642. https://doi.org/10.1002/pro.3566.

70. Conchillo-Solé, O., de Groot, N.S., Avilés, F.X., Vendrell, J., Daura, X., Ventura, S., (2007). AGGRESCAN: a server for the prediction and evaluation of "hot spots" of aggregation in polypeptides. *BMC Bioinf.* **8**, 65. https://doi.org/10.1186/1471-2105-8-65.

71. Emily, M., Talvas, A., Delamarche, C., (2013). MetAmyl: A META-Predictor for AMYLoid Proteins. *PLoS One* **8**, e79722.

72. Munir, F., Gul, S., Asif, A., Minhas, F.A., (2021). MILAMP: Multiple Instance Prediction of Amyloid Proteins. *IEEE/ACM Trans. Comput. Biol. Bioinf.* **18**, 1142–1150. https://doi.org/10.1109/tcbb.2019.2936846.

73. Walsh, I., Seno, F., Tosatto, S.C.E., Trovato, A., (2014). PASTA 2.0: an improved server for protein aggregation prediction. *Nucleic Acids Res.* **42**, W301–W307. https://doi.org/10.1093/nar/gku399.

74. Meisl, G., Kirkegaard, J.B., Arosio, P., Michaels, T.C.T., Vendruscolo, M., Dobson, C.M., Linse, S., Knowles, T.P.J., (2016). Molecular mechanisms of protein aggregation from global fitting of kinetic models. *Nature Protoc.* **11**, 252–272. https://doi.org/10.1038/nprot.2016.010.

75. O'Toole, G.A., Kolter, R., (1998). Flagellar and twitching motility are necessary for Pseudomonas aeruginosa biofilm development. *Mol. Microbiol.* **30**, 295–304.

76. Schindelin, J. et al, (2012). Fiji: an open-source platform for biological-image analysis. *Nature Methods* **9**, 676–682. https://doi.org/10.1038/nmeth.2019.